Noname manuscript No.
(will be inserted by the editor)

Ocean versus atmosphere control on western European wintertime temperature variability

Ayako Yamamoto · Jaime B. Palter · M. Susan Lozier · Michel S. Bourqui · Susan J. Leadbetter

Received: date / Accepted: date

Abstract Using a novel Lagrangian approach, we assess the relative roles of the atmosphere and ocean in setting interannual variability in western European wintertime temperatures. We compute sensible and latent heat fluxes along atmospheric particle trajectories backtracked in time from four western European cities using a Lagrangian atmospheric dispersion model driven with meteorological reanalysis data. The material time rate of change in potential temperature and the surface turbulent fluxes computed along the trajectory show a high degree of correlation, revealing a dominant control of ocean-atmosphere heat and moisture exchange in setting heat flux variability for atmospheric particles en route to western Europe. We conduct six idealised simulations in which one or more aspects of the climate system is held constant at climatological values and these idealised simulations are compared with a control simulation, in which all components of the climate system vary realistically. The results from these idealised simulations suggest that knowledge of atmo-

A. Yamamoto · J. B. Palter · M. S. Bourqui
Department of Atmospheric and Oceanic Sciences
McGill University
Montréal, Canada
E-mail: ayako.yamamoto@mail.mcgill.ca

M. S. Lozier
Division of Earth and Ocean Sciences
Nicholas School of the Environment
Duke University
Durham, North Carolina, USA

M. S. Bourqui
Dr Bourqui - Atmospheric and Climate Sciences Consulting
Zurich, Switzerland
Department of Physics
Université de Montréal, Montréal, Canada

S. J. Leadbetter
Met Office, Exeter, UK

spheric pathways is essential for reconstructing the interannual variability in heat flux and western European wintertime temperature, and that variability in these trajectories alone is sufficient to explain at least half of the internannual flux variability. Our idealised simulations also expose an important role for sea surface temperature in setting decadal scale variability of air-sea heat fluxes along the Lagrangian pathways. These results are consistent with previous studies showing that air-sea heat flux variability is driven by the atmosphere on interannual time scales over much of the North Atlantic, whereas the SST plays a leading role on longer time scales. Of particular interest is that the atmospheric control holds for the integrated fluxes along 10-day back trajectories from western Europe on an interannual time scale, despite that many of these trajectories pass over the Gulf Stream and its North Atlantic Current extension, regions where ocean dynamics influence air-sea heat exchange even on a very short time scale.

Keywords Air-sea interaction · Lagrangian method · climate variability

1 Introduction

Wintertime average surface air temperatures in western Europe are warmer than the zonal mean at the equivalent latitude by up to 15 K (Figure 1). The cause of this relative warmth has traditionally been attributed to poleward ocean heat transport by the Gulf Stream extension and its subsequent heat release to the atmosphere (Maury 1860). A study by Seager et al (2002) challenged the traditional view of ocean heat transport's central role in mild winters in Europe, and offered the alternative hypothesis that the zonal asymmetry in wintertime temperature is predominantly caused by stationary waves set by orographic forcing, with the annually-integrated net ocean heat transport convergence playing only a marginal role. This alternative argument posits that orographic forcing by the Rockies produces predominantly northwesterly winds over the western side of the North Atlantic basin and southwesterly winds over the eastern side. While the former brings cold continental air masses to northeastern United States, the latter brings warm maritime air masses to western Europe, thereby creating the zonal asymmetry in temperature. Although air mass pathways play a critical role in setting variability in climate, the exact balance of processes setting wintertime European climate remains an active area of debate (Rhines et al 2008).

Importantly, neither the paradigm that sees ocean heat transport as the cause of Europe's mild temperatures nor the one that poses a more central role for air mass trajectories addresses the

question of what controls western European climate variability. Much recent work has exposed the relative contributions of the ocean and atmosphere in setting heat flux variability over the North Atlantic, which ultimately influences climate variability in Europe. Dong et al (2007) showed that in the Gulf Stream region, variability in upper-ocean heat content, which is predominantly due to ocean heat transport convergence (Dong and Kelly 2004), is positively correlated with heat fluxes to the atmosphere on interannual to decadal time scales. A similar conclusion has been drawn over the Kuroshio extension region in the Pacific (Yasuda and Hanawa 1997), and this heat flux in turn has been found to significantly impact the overlying atmospheric temperature via the perturbation of the surface layer heat budget (Yulaeva et al 2001). On the other hand, over the mid-latitude North Atlantic basin interior, Bjerknes (1964) surmised that air-sea heat flux variability is driven by the atmosphere on interannual and shorter time scales, while the ocean is a major driver only on a longer, multidecadal time scale. Gulev et al (2013) provided evidence in support of this conjecture using century-long observational datasets by showing that sea surface temperature (SST) and turbulent fluxes are anti-correlated on interannual time scales and positively correlated on multidecadal time scales, thereby suggesting a transition between an atmospheric control over turbulent fluxes at short time scales to an oceanic control at longer time scales. Buckley et al (2014) further confirmed that on the interannual time scales that are well-represented in an ocean reanalysis product (Wunsch and Heimbach 2007) heat flux variability is principally controlled by the atmosphere over most of the North Atlantic outside the Gulf Stream region, while the oceanic convergence of heat is critical in the Gulf Stream region.

Because air masses, on their way to western Europe, frequently cross over both the Gulf Stream and the non-Gulf Stream part of the basin, it is not clear whether the ocean or the atmosphere controls the accumulation of heat along the trajectory. This question is therefore ideally addressed in a Lagrangian framework. Previous studies attempted to answer related questions using an Eulerian approach and statistical models (e.g., Blender et al 2003; Gámiz-Fortis et al 2011; Junge and Stephenson 2003), and generally found that knowledge of SST variability yields little predictive skill for European climate on interannual time scales.

Our underlying question of how air mass pathways and ocean heat transport contribute to European climate is timely, given recent observational evidence of large interannual variability in the mass and heat transport of the Atlantic Meridional Overturning Circulation (AMOC; McCarthy et al 2012), much of which manifests as changes in Gulf Stream transport. For instance, in 2009 a

30% decline of AMOC transport robbed the North Atlantic north of 26°N of over 0.3 PW (1 PW = 10^{15} W). Given that as much as half of the total meridional transport of heat is carried by the ocean at this latitude (Trenberth and Caron 2001) and that 90% of the oceanic meridional heat transport in the North Atlantic is due to the AMOC (Johns et al 2011), one might expect this substantial AMOC reduction to result in a decline in the ocean to atmosphere heat exchange to the north of 26°N.

Our goal is to relate wintertime temperature variability in four western European cities to the pathways Lagrangian particles in the atmosphere follow before arriving in each of these cities, and the oceanic and atmospheric state they see along that pathway. In order to do so, we trace three-dimensional air mass trajectories backwards in time from the surface of these four cities, and calculate the air-sea heat fluxes along the pathways. Because turbulence in the planetary boundary layer (PBL) creates an envelope of possible pathways with a common end point, a Lagrangian atmospheric dispersion model is used to characterise the distribution of likely trajectories. We then vary, in turn, these trajectory distributions, the atmospheric properties along them, and the oceanic properties beneath them, in order to explore the degree of control each of these factors has on the total heat and moisture a parcel gains or loses en route to Europe. In the next section we describe the Lagrangian dispersion model (Section 2.1), the bulk formulae used to calculate turbulent fluxes along the particle pathways (Section 2.2), the Lagrangian heat budget and the critical role of the turbulent fluxes in setting variability in this budget (Section 2.3), and the idealised simulations used to explore the source of variability in these fluxes (Section 2.4). In Section 3, the results of these idealised simulations are compared against a control simulation to expose the sensitivity of the along-trajectory heat fluxes to various aspects of ocean and atmosphere variability. Conclusions and an outlook for the future are offered in Section 4.

2 Methodology

2.1 Establishing air parcel trajectories with FLEXPART

The Lagrangian particle dispersion model FLEXPART (Stohl et al 2005) version 9.02 is used to backtrack the air flow from the surface of four locations in western Europe. FLEXPART is one of the most widely-used dispersion models for various atmospheric transport applications. Unlike kinematic trajectory models, FLEXPART includes subgrid-scale convection and turbulence that

are essential in simulating boundary layer motion, and as such, it is an appropriate tool for the purposes of the current study.

In FLEXPART, each trajectory is calculated as follows:

$$\mathbf{X}(t + \triangle t) = \mathbf{X}(t) + \mathbf{v}(\mathbf{X}, t) \triangle t, \tag{1}$$

where t is time, $\triangle t$ is the time increment, $\mathbf{X}$ is the position vector, and $\mathbf{v} = \bar{\mathbf{v}} + \mathbf{v}_t + \mathbf{v}_m$, is the three-dimensional wind speed vector comprised of grid scale wind ($\bar{\mathbf{v}}$), turbulent wind fluctuations ($\mathbf{v}_t$), and the mesoscale wind fluctuations ($\mathbf{v}_m$). The addition of the last two terms to simulate the effect of turbulent motion is what makes this dispersion model different from kinematic trajectory models, which account only for the resolved grid scale winds. Turbulent motions are included by adding a perturbation to the velocity field for air parcels in the PBL, where these random motions are calculated by solving Langevin equations for Gaussian turbulence (Stohl and Thomson 1999). Mesoscale velocity, whose spectral interval falls between the resolved flow and the turbulent flow, is approximated by solving an independent Langevin equation following Maryon (1998). Additionally, the PBL height at each particle's hourly position is diagnosed by using the Richardson number criterion for stability and a lifting-parcel technique (Vogelezang and Holtslag 1996).

In the current study, FLEXPART is forced with the hourly Climate Forecast System Reanalysis (CFSR) forecast and reanalysis datasets from National Centers for Environmental Prediction (NCEP; Saha et al 2010), with horizontal resolution of 0.5° and 37 vertical levels, from 1981 to 2009. After its release, each particle is advected backwards in time by the three-dimensional gridded wind from NCEP CFSR plus the turbulent and mesoscale velocities described above, linearly interpolated to the particle's position. Additional atmospheric quantities such as temperature, specific humidity and air density are also interpolated to the particle's position at each time step, useful for tracking the material rate of change in temperature and diagnosing the air-sea heat fluxes. We acknowledge that every reanalysis product has its limitations, and NCEP CFSR product is no exception (e.g., Decker et al 2012). However, because the focus of the current study is to understand the processes setting the variability in air-sea heat exchange, rather to focus on a single event or the exact size of the fluxes, we believe that our main conclusions should not be particularly sensitive to the product used.

The four different locations in western Europe selected as end points (i.e., "release" points for the backward trajectories) are populous cities separated by approximately 5° of latitude: Dublin (53.20° N 6.15° W), Paris (48.87° N, 2.34° E), Toulouse (43.60° N, 1.44° E), and Lisbon (38.70° N, 9.18° W). The three northern cities have pronounced interannual wintertime temperature variability with the maximum range exceeding 10°C in Paris, while Lisbon displays the most stable year-to-year temperatures (Figure 2). Every January from 1981 to 2009, 50 particles totalling 1 kg of air mass are released from the surface at each location twice daily at 0 UTC and 12 UTC from January 10 to 31 for the duration of 10 days backward in time. January is the month with the largest zonal temperature anomalies in Europe, and thus the time period is chosen to exclusively and thoroughly sample January air mass pathways. Thus, the total number of atmospheric particles released is 60,900 particles (50 particles/release × 2 release/day × 21 days/January × 29 Januaries) for each city.

Number density plots of the particle trajectories for each city are shown in Figure 3. We visually compared our number density plots (Figure 3) with the cyclone climatologies (Hodges et al 2011; Tilinina et al 2013) and confirmed that the densest pathways generally correspond to the climatological cyclone track. Expected differences between our number density plots and these cyclone climatologies arise because we track particles backwards from several locations which are not necessarily downstream of the cyclone track, and also because the particles are not filtered by any means, while the computation of the storm track requires band-pass filtering.

The choice of the number of particles to be released was determined based on statistics of particle positions: Increasing the number of releases from 50 to 500 had little influence on the mean particle positions at every time step (i.e. the mean position from a 50 particle release is within ± 3 degree latitude of the mean position of a 500 particle release at every time step). Likewise, the size of the envelope of trajectories does not grow considerably when more particles are released: The time mean standard deviation for any particle number greater than 20 is within ±0.5 degree latitude of the standard deviation for 500 particles. Thus, we conclude that 50 back-tracked particles sufficiently sample the envelope of the air mass pathway spatial extent at a reasonable numerical cost. The 10-day duration for back trajectories was chosen so that diabatic exchange along the length of the trajectory has a sufficient amount of time to considerably alter the initial temperature of the parcel. Indeed, the autocorrelation function of potential temperature (Figure 4) suggests a Lagrangian decorrelation time scale (taken here as the first zero-crossing of the autocorrelation) of

about 3 days. Thus, the memory of a particle's initial temperature is erased over the course of its 10-day trajectory and it arrives in its destination city after being strongly influenced by diabatic processes.

2.2 Bulk Formulae

The oceanic influence on the atmosphere is communicated through turbulent fluxes at the air-sea interface. We diagnose these fluxes using TOGA-COARE bulk air-sea algorithm version 3.0a (Fairall et al 1996, 2003), applied along each trajectory's hourly position whenever particles lie within PBL over the ocean. Approximately 25% of all hourly output points fall within PBL (see schematic in Figure 5). Our assumption is that the surface turbulent fluxes influence the entire air mass in the PBL due to the turbulent mixing.

In the COARE bulk formulae (Fairall et al 1996), sensible heat (SH) and latent heat (LH) fluxes are calculated as follows by the ocean-atmosphere gradient of temperature and specific humidity, respectively:

$$SH = \rho_a c_{pa} C_{sh} S(T_s - \theta_a) \tag{2}$$

$$LH = \rho_a L_e C_{lh} S(q_s - q_a), \tag{3}$$

where C_{sh} and C_{lh} are the transfer coefficients for SH and LH, respectively; ρ_a is the air density; S is the wind speed relative to the ocean current; c_{pa} is the atmospheric isobaric heat capacity; L_e is the latent heat of evaporation; T_s is the sea surface interface temperature; θ_a is the atmospheric potential temperature; q_s is the interfacial water vapour mixing ratio; and q_a is the atmospheric water vapour mixing ratio. We compute q_s from the saturation mixing ratio at T_s for pure water, and then multiply by a factor of 0.98 to account for the reduction of vapour pressure due to the sea surface salinity. Note that the atmospheric parameters T_a and q_a are taken at the reference height of 2 m in this study, which is adjusted to a fixed height of 10 m within the bulk formulae.

The principal controls on the turbulent flux variability are the temperature gradient for SH and the humidity gradient for LH, with the dependency on the relative wind speed, S, playing a secondary role. These variables are obtained by interpolating the data provided by hourly NCEP datasets to the particle's hourly 2D location, having projected from the 3D position to

the ocean/atmosphere interface. Several variables (the transfer coefficients, interface water vapour mixing ratio, and the wind speed relative to the ocean current) are computed within the COARE algorithm from the native variables provided by NCEP.

Our sign convention is such that SH and LH are directed from the ocean to the atmosphere. Thus, SH is positive whenever the ocean surface is warmer than the air passing over. Likewise, LH is positive whenever the atmosphere is moistened by its interaction with the ocean. In fact, LH is only negative when the overlying atmosphere is both warmer than the SST beneath and saturated, which is very rare in the winter. Thus, LH is almost always greater than or equal to zero, and a parcel passing over the ocean normally gains LH. It is important to bear in mind that LH is not a direct measure of heat exchanged; rather, it is an indication of a gain or loss in the internal energy of the air parcel due to a change in its humidity. Only upon condensation of the moisture gained, possibly at a great distance from the LH flux, will an air parcel be heated. To facilitate a direct comparison to the SH flux, we convert the LH to the temperature change induced in the parcel upon total condensation of the moisture gained.

We recognise some caveats arising from our use of bulk formulae: They are validated to be accurate within 10% for wind speeds up to 20 m/s, and can be calculated only over the ocean (Fairall et al 2003). Furthermore, here we use the same treatment over sea ice, although atmosphere-ice interaction qualitatively and quantitatively differs from ocean-atmosphere interaction. However, because our calculated trajectories are in contact with sea ice only approximately 1% of the time, with the bulk calculation overestimating the heat flux by about 50% for SH and 20% for LH on average during these times, this caveat introduces a trivial error. To check the influence of this simplification on the fluxes, we compared the 10-day integrated heat fluxes (SH + LH) along the atmospheric pathways computed by bulk parametrisation with the 10-day integrated heat fluxes that are obtained by interpolating the heat fluxes provided by NCEP CFSR datasets along the same particle trajectories. In all cities, in all years, and for both latent heat and sensible heat flux, the mean estimate from the bulk parametrisation is not significantly different from the mean of the interpolated fluxes based on a student t-test, thus justifying the usage of bulk formulae in turbulent flux computations.

2.3 Lagrangian heat budget

The Lagrangian time rate of change in potential temperature is driven by the heat fluxes along the trajectory of an atmospheric particle, according to the following equation:

$$\int \frac{D\theta}{Dt} dt = \theta_{final} - \theta_{initial} = \int \frac{QA}{mc_p} dt, \tag{4}$$

where, $\theta_{initial}$ and θ_{final} are the initial and final (endpoint) potential temperatures of the particles, respectively, A is the area occupied by the atmospheric particle, m is the mass of the atmospheric particle, and c_p is the atmospheric specific heat (1004 J K^{-1} kg^{-1}). Following Peixoto and Oort (1992), the diabatic heating term of Q is defined as

$$Q = \text{diabatic heating} = Q_{radiative} + Q_{sensible} + Q_{latentrelease}, \tag{5}$$

where $Q_{radiative}$ is the net radiative heating term due to shortwave and longwave radiation, $Q_{sensible}$ is sensible heating in the planetary boundary layer, and $Q_{latentrelease}$ is the heat gained (lost) upon condensation (evaporation) of water vapour (liquid water). Additional terms in the heat budget arise from the use of parametrisations of subgrid-scale processes in the CFSR reanalysis, including convection and vertical diffusion. $Q_{radiative}$ is obtained by interpolating the heating rate due to the CFSR shortwave and longwave radiation at the three-dimensional position of each particle. Likewise, heating due to convection and vertical diffusion are interpolated to the particle position.

In order to set up the idealised simulations described next in Section 2.4, we calculate $Q_{sensible}$ from bulk formulae. On the other hand, $Q_{latentrelease}$ cannot be quantified using bulk formulae alone, because $Q_{latentrelease}$ is the actual heat gain (loss) due to the condensation (evaporation) of moisture in the particle. Heat in the Lagrangian particle is consumed when cloud droplets evaporate and is released when clouds form. Neither of these processes necessarily occur locally in the region where air-sea latent heat fluxes occur, as quantified by the the calculation of LH. Thus, we cannot directly calculate $Q_{latentrelease}$ along the particle trajectories from bulk parametrisation, nor close the heat budget exactly.

Despite this caveat, the vast majority of the variability in along-path potential temperature change ($\int \frac{D\theta}{Dt} dt$) arises from variability in the accumulated surface turbulent fluxes solved by bulk

parametrisation ($\int(SH + LH)dt$) alone, as shown in the first column of Table 1. Indeed, including heating due to radiation, convection, and vertical diffusion does not increase the correlation with $\int \frac{D\theta}{Dt}dt$. Likewise, replacing LH with the term large scale condensate heating, provided by CFSR, does not increase the correlation. However, including all of the available heating terms and approximating $Q_{latentrelease}$ with large scale condensate heating does bring the budget closer to closure. Nonetheless, the correlations in Table 1 suggest that turbulent exchange with the ocean dominantly sets atmospheric heat and moisture content variability. This dominance gives us confidence to proceed with idealised simulations in which the heat fluxes are calculated by bulk formulae while manipulating either oceanic or atmospheric properties.

The second column of Table 1 indicates that the initial temperature of a particle plus the heating estimated from bulk parametrised fluxes ($\int(SH + LH)dt + \theta_i$) is also significantly correlated with the final potential temperature in the European cities. This correlation coefficient is slightly lower than the correlation between $\int \frac{D\theta}{Dt}dt$ and the accumulated turbulent fluxes, $\int(SH+LH)dt$, because the initial potential temperature is anti-correlated with the surface turbulent fluxes (the correlation ranges from -0.43 to -0.75, not shown). This anti-correlation indicates that the colder the initial temperature of a particle, the more heat it gains and vice versa, an expected consequence of the dependence of heat fluxes on the air-sea temperature gradient. The correlations between θ_f and the sum of θ_i and the heating terms are barely changed by the addition of the radiation term to the turbulent fluxes (on average increase of the correlation coefficient by 0.04) or the other known heating terms (average decrease of 0.13).

2.4 Idealised simulations

The NCEP reanalysis fields, the atmospheric particle trajectories from the FLEXPART model, and the bulk formulae provide the building blocks for a suite of idealised Lagrangian simulations. In these simulations, sensible and latent heat fluxes are calculated along each FLEXPART trajectory while holding one or more factor determining these heat fluxes constant, thereby creating a framework for separating the influence of oceanic and atmospheric variability on total heat flux variability. We compare the results of these six idealised simulations with the result of a control simulation (*Control*), which is integrated using both true-state oceanic and atmospheric variability. Thus, *Control* includes all the inherent coupled behaviour of the ocean-atmosphere system. A

detailed description of each simulation is given below, and a brief synopsis of the simulation design is given in Table 2.

PathVAR simulation

In this simulation, we allow atmospheric particle trajectories and wind speed to vary realistically, while holding the turbulent fluxes at fixed climatological values. To fix the fluxes at their climatological values, we compute the turbulent fluxes using bulk parametrisation along varying pathways, but with the 29-year average of SST, surface atmospheric temperature (T2m) and humidity at 2 m above sea level (q2m), shown in Figure 6. Thus, the heat flux variability in this simulation arises solely due to dynamic variability in the atmosphere, without any variability caused by variability in T2m, q2m and SST.

FluxVAR simulation

The *FluxVAR* simulation is the reverse of the *PathVAR* simulation: Here turbulent fluxes vary realistically, but the atmospheric particle trajectories are held fixed. Thus, this simulation reveals the heat flux variability due entirely to variability in T2m, q2m and SST, and ignores variability in atmospheric particle trajectories, except to the degree that the T2m, q2m and SST reflect the variable pathway trajectories in the reanalysis data.

To select a set of unvarying particle trajectories, we randomly pick 50 trajectories from all years and particle releases, such that we do not introduce any daily variability. Along these unvarying 50 trajectories, bulk parametrised fluxes are computed at every time step with the varying T2m, q2m and SST. We then repeat this process 10 times, each time by picking a different random set of 50 trajectories, thereby creating a spread of heat fluxes for the *FluxVAR* simulations that can be compared against *Control*. In total, 500 particle (50 particles $\times$ 10 realisations) are selected for each city. The mean correlation coefficient of *FluxVAR* with *Control* stabilises after approximately 5 realisations; we thus conclude that 10 realisations of 50 random trajectories provide ample sampling of the full range of possible pathways. The resultant spatial distribution of these 10 realisations of 50 randomly selected unvarying pathways are very similar to what is shown in Figure 3 for the full set of trajectories, without any visible bias (not shown).

AtmVAR simulation

Here, we compute the bulk parametrised fluxes with fixed climatological mean SST, but with the varying atmospheric state, which includes realistic trajectories, wind speeds, T2m, and q2m.

This simulation aims to isolate the role of the atmosphere in determining the turbulent flux variability.

SSTVAR simulation

This simulation is the opposite of the *AtmVAR* simulation. For *SSTVAR*, we calculate the bulk parametrised fluxes with the varying SST and ocean current speeds, but hold fixed all the atmospheric particle trajectories and the atmospheric state variables. The same set of unvarying atmospheric pathways as in *FluxVAR* is utilised, and the 29-year mean atmospheric state (T2m, q2m and the wind speed) is interpolated to the 2D location of the hourly particle positions. This simulation aims to isolate the role of the ocean state in setting the turbulent flux variability. Note that since ocean currents are normally two orders of magnitude smaller than the atmospheric wind speeds, the parameter S in bulk formulae is largely dominated by the atmospheric wind. Thus, the ocean role investigated here stems almost exclusively from the SST variability.

PathSSTVAR simulation

In this simulation, the fluxes are calculated with varying SSTs, pathways, and wind speed, while holding the T2m and q2m at their January, 29-year climatological mean values. Thus, this simulation reveals the degree to which the fluxes are influenced by particle trajectories and SST alone.

SATVAR simulation

Here, the fluxes are calculated along fixed pathways and with fixed SST and winds, but with varying T2m and q2m above the sea surface. The unvarying pathways used here are the same as the ones used in *FluxVAR* and *SSTVAR* simulations. Therefore, the resultant heat flux variability in this simulation is solely attributable to the T2m and q2m variability.

Note that those variables that are not specified in the explanation of each simulation above but are required for the bulk formulae (surface long and short radiation, precipitation rate, and surface pressure) are set to vary realistically in each simulation. It is important to bear in mind that atmospheric and oceanic variability are in reality tightly linked with one another. By testing every combination of fixed and variable climate factors in the idealised simulations and comparing the results carefully with that of *Control*, we also aim to gain insight into these coupled links.

3 Results and Discussion

3.1 Results and discussion of the six idealised simulations

The results of the six idealised simulations described in Section 2.4 are compared to the *Control* simulation in order to investigate the factors driving heat flux variability for atmospheric particle trajectories en route to western Europe. The comparison is summarised in Figure 7, and the corresponding correlation coefficients and the root mean square errors are given in Table 3 and Table 4, respectively.

The salient message from these results is unequivocal: Knowledge of the atmospheric pathways is most important in determining the interannual variability in along-path air-sea heat and moisture exchange, as can be seen from comparison between the simulation results which have realistically varying pathways (*PathVAR*, *AtmVAR*, and *PathSSTVAR*) and the ones with fixed pathways (*FluxVAR*, *SSTVAR*, and *SATVAR*).

In particular, *PathVAR* and *AtmVAR* capture most of the variability seen in *Control*. Adding information about the atmospheric temperature and humidity increases agreement with *Control*: *AtmVAR* has the smallest root mean square error compared to *Control* of all the simulations (Table 4). Yet, surprisingly the correlation coefficients of *AtmVAR* are slightly lower for the two northern cities (Dublin and Paris) and only marginally higher for the southern ones, compared to those from *PathVAR* (Table 3). Why does including T2m and q2m variability fail to significantly improve these correlations? Figure 7 suggests the answer to this conundrum: Before 1996, the heat fluxes from the *AtmVAR* simulation are biased high, whereas after 1996 they are biased low. This shifting bias is likely caused by a basin-scale SST increase starting in 1996 that outpaced the longer-term linear trend, a change which has been attributed either to a shift from negative to positive phase of the Atlantic Multidecadal Oscillation (AMO) (Sutton and Dong 2012), or to changes in net radiative forcing (e.g., Booth et al 2012). Given the expectation that the ocean exerts a dominant control on air-sea heat flux variability on decadal time scales (Gulev et al 2013), the transition around 1996 from low to high SST would cause a shift from reduced to enhanced fluxes and from lower to higher T2m. However, when these warming T2m and fixed SSTs are fed into the bulk formulae in *AtmVAR*, they cause a reduction of the fluxes over time. Indeed, by eliminating the influence of the decadal shift by calculating the correlation coefficients for the first and last decades alone, the correlation coefficients between *AtmVAR* and *Control* on interannual time scale

increase significantly, surpassing the correlation between *PathVAR* and *Control*. This aspect of the results suggests that SST influences along-pathway heat flux variability on decadal timescales, with implications for northwestern European wintertime climate variability.

Similarly, the correlation between *PathSSTVAR* and *Control* is much weaker than between *PathVAR* and *Control*, despite that the *PathSSTVAR* simulation accounts for realistically varying SSTs in addition to pathways. A solution to this puzzle is that the atmosphere drives surface turbulent fluxes over much of the ocean on sub-decadal time scales (Buckley et al 2014), thereby creating interannual SST anomalies (Gulev et al 2013). In such a regime, a year with anomalously large fluxes creates anomalously low SSTs and vice versa. However, in *PathSSTVAR*, the SST varies realistically while T2m and q2m are constant; thus, in a low SST year, the heat flux calculated via bulk parametrisation is also low, the reverse of what is expected in reality when the atmosphere drives the fluxes. Therefore, we interpret the slightly weaker correlations in *PathSSTVAR* to be consistent with this atmospheric control on interannual time scales.

Another striking feature in Figure 7 is that both *PathVAR* and *FluxVAR* underestimate the total accumulated flux relative to *Control*. The lower accumulated heat fluxes in the *PathVAR* and *FluxVAR* simulations relative to *Control* reflect the fact that atmospheric particle trajectories and the fluxes along them are, in reality, tightly linked, and cutting these linkages leads to systematically lower total fluxes. Evidence in support of the importance of this coupling is provided by examining trajectory positions, T2m, and SST anomalies associated with the years when *PathVAR* most strongly underestimates the true turbulent fluxes (Figure 8). The maps in Figure 8 reveal that the years when *PathVAR* most strongly underestimates the true fluxes are years in which pathways take an anomalously long and northerly route, originating over the cold North American continent and the Labrador Sea (Figure 8a). In these years, anomalously low T2m is advected along those pathways, while SST is close to its climatological mean values (Figure 8b and c). This cold air advection produces larger turbulent fluxes in reality (and, therefore, in *Control*). Thus, when this link between the particle pathways and T2m is cut (as in *PathVAR* and *FluxVAR*), the turbulent fluxes are strongly underestimated. It is interesting to note that the years shown in Figure 8 are those years with the largest along-trajectory accumulated fluxes in *Control*. Therefore, the atmospheric particles that take an anomalously northern route to Europe gain the most heat along their journey. The link between pathways and fluxes holds true for both anomalously high and low fluxes: for example, just as northerly pathways advect cool air with them and lead to high

fluxes (Figure 8), anomalously southerly pathways can lead to low fluxes along the trajectories (not shown).

As an additional exploration of the link between pathway anomalies and flux anomalies, we compare the heat fluxes averaged over the pathways of the air parcels that arrive in Dublin for all 29-year releases ($\overline{F_{traj}}$, Figure 9a) and the standard Eulerian 29-year mean heat fluxes ($\overline{F}$, Figure 9b). The difference between these two fields (Figure 9c) clearly suggests that particles tracked backwards from Europe sample some regions of the ocean preferentially during times of anomalous heat flux. Regions visited by particles during anomalously low flux times are found south of about 30°N (Figure 9c, where $\overline{F_{traj}}$ is lower than $\overline{F}$). In contrast, particles see high flux anomalies along the Gulf Stream and over the Labrador and Irminger Seas (Figure 9c, where $\overline{F_{traj}}$ is greater than $\overline{F}$). At any given particle position, the hourly flux along a Lagrangian particle is about equally likely to be larger or smaller than the climatological flux in a given grid cell (Figure 9d). However, because the air-sea flux distributions are positive-skewed, the magnitude of the difference (F_{traj} - $\overline{F}$) is about 50% larger when averaged over all hourly positions during which $F_{traj} > \overline{F}$ than when $F_{traj} < \overline{F}$ (Figure 9d). In other words, because the true path/flux covariability is contained in the *Control* simulation, it better samples the anomalous fluxes of both signs than the idealised simulations. The better-sampled extremes in *Control* lead to systematically higher January-mean fluxes than in *PathVAR* and *FluxVAR*, because the distribution of the fluxes is strongly positive-skewed.

The importance of path/flux covariability is also confirmed by *AtmVAR*, in which both trajectories and T2m vary realistically, and only SST is held constant (Figure 7, middle column). In *AtmVAR*, the amplitudes of the fluxes closely match those of the *Control* simulation and have no systematic bias.

In sum, the idealised simulations suggest that heat flux interannual variability is dominantly set by the trajectories of the Lagrangian atmospheric particles as can be seen from the high degree of fidelity between *Control* and *PathVAR*, *AtmVAR*, and *PathSSTVAR*. Knowledge of realistically varying pathways alone allows the reconstruction of no less than 72% of the heat flux variability. In contrast, knowledge of the SST variability alone is not useful for predictability of air-sea heat exchange along the Lagrangian pathways on interannual time scales. However, SST warming over the 29-year climatology does influence the accumulated heat fluxes on decadal time scales.

3.2 *UniformSST* simulation

Though the results in Section 3.1 suggest that temporal SST variability is not a major driver of interannual flux variability, they do not reveal the role of spatial variability in SST. We hypothesise, for example, that in years where the atmospheric trajectories predominantly travel over the warm Gulf Stream, the surface fluxes would be higher than in years when the pathway is over the cool subpolar ocean. Therefore, we perform one additional simulation, where we allowed true variability of the atmospheric state (as in *AtmVAR*), but held the ocean temperature everywhere at a uniform value (*UniformSST* simulation; Figure 10). This assigned value is the mean SST sampled by the atmospheric particles backtracked from each city: 7.5°C for Dublin, 7.3°C for Paris, 9.4°C for Toulouse, and 11.8°C for Lisbon. Setting the SST to a uniform value everywhere diminishes the degree of correlation with the *Control* simulation by 23% on average relative to the original *AtmVAR* simulation. Interestingly, the strength of the correlation between heat fluxes in *UniformSST* and the *Control* simulation is generally higher than that of *PathSSTVAR* (compare correlation coefficients given in Figure 10 with Table 3). The agreement in variability between *UniformSST*, *AtmVAR* and *Control* suggests that interannual surface flux variability is principally driven by the variability in air temperature and humidity wherever the parcels travel, and secondarily by the spatial patterns in SST along those pathways.

4 Conclusions

In this study, we have presented a novel method to investigate the mechanisms driving temperature variability in western Europe, in which air-sea turbulent fluxes are summed along the Lagrangian back trajectories of atmospheric particles travelling to several European cities while holding one or more component of the climate system constant. For all but one of the cities we investigated, variability in these accumulated heat fluxes accounts for a majority of the variability in the winter temperatures. Thus, our framework helps uncover the relative importance of variability in SST and atmospheric dynamics and thermodynamics in setting western European winter temperature variability. The Lagrangian framework is especially valuable because atmospheric particles travelling to Europe generally pass over both the Gulf Stream, where ocean heat transport convergence is known to play an active role in setting air-sea heat exchange on all time scales (Buckley et al 2014; Dong and Kelly 2004; Dong et al 2007), and the basin interior, where variability in the ocean is

only expected to significantly influence air-sea heat exchange on time scales of decades and longer (Bjerknes 1964; Buckley et al 2014; Gulev et al 2013).

A principal insight from this suite of Lagrangian simulations is that knowledge of atmospheric particle trajectories alone is sufficient for understanding much of the interannual variability in wintertime heat fluxes accumulated along parcels en route to western Europe. However, surface air temperature and moisture and SST along the trajectories are also essential to understanding winter climate in Europe. First, the pathway a particle takes to Europe and the temperature and moisture along that pathway are linked, such that using a climatological estimate of either variable leads to an underestimate of the accumulated flux. This linkage is most clearly demonstrated in years when the trajectories are anomalously northerly and advect cold, dry, continental air from North America, triggering large ocean to atmosphere turbulent fluxes. Second, a decadal-scale shift in SST discernibly influences the accumulation of heat for atmospheric particles travelling to Europe. Therefore, using a climatological SST to calculate air-sea turbulent fluxes misses this source of low frequency variability.

One surprising conclusion from our simulations is that interannual variability in heat fluxes accumulated along the Lagrangian trajectories to Europe is only moderately influenced by spatial variations in SST. At the outset of this work, we hypothesised, for example, that a year with a preponderance of Lagrangian trajectories passing over the warm Gulf Stream extension would correlate with larger heat fluxes in that year. We tested this hypothesis by running a simulation that held SST at a constant and uniform value over the entire North Atlantic. This simulation yielded flux estimates that were still highly correlated with the true fluxes as were those from a simulation that used a spatially-varying, climatological mean value for SST. This test clarified that the spatial variations in SST are subdominant in setting the interannual variability in accumulated heat fluxes.

In summary, on subdecadal time scales, variability in winter European temperatures is principally controlled by variability in the atmosphere. Although ocean dynamics in the Gulf Stream and North Atlantic Current may influence high frequency variability in air-sea exchange locally, this influence is not apparent in the total accumulated heat flux for particles travelling to Europe or the associated winter temperatures upon arrival. Our findings that the biggest fluxes occur in the Gulf Stream region but these fluxes do not strongly manifest in downwind climate variability in Europe is in harmony with the fact that, although the Gulf Stream region is a major oceanic

cyclone genesis region, it is only a minor contributor to the advected moisture in Europe (Rudeva and Gulev 2011). Our synthesis also suggests that high-frequency variability in AMOC, such as the observed decline in 2009 (McCarthy et al 2012), is unlikely to manifest as a drop in western European temperature unless accompanied by a change in atmospheric trajectories. However, we show that the well-documented North Atlantic-wide SST shift to higher temperatures in 1996, commonly associated with the Atlantic Multidecadal Oscillation (e.g., Alexander et al 2014; Enfield et al 2001; Sutton and Dong 2012) noticeably influences the strength of winter air-sea heat exchange accumulated along Lagrangian parcels travelling to Europe.

It is therefore intriguing that previous studies have failed to find any influence of the AMO on wintertime European climate (Arguez et al 2009). Anomalous SST associated with the AMO is thought to drive changes in the storm track over the North Atlantic (Dong et al 2013; Häkkinen et al 2011; Kushnir 1994; Woollings et al 2012), although the mechanisms leading to deflection of the storm track are complex and not fully understood (e.g., Orlanski 1998). If AMO variability does cause such deflection, both the particle pathways and the turbulent fluxes linked to the underlying SST would vary in a coordinated fashion in response to the AMO. We hypothesise that this coupling could suppress the wintertime manifestation of the AMO in western European temperatures. Thus, in a follow-up study, we evaluate this hypothesis with an extension of the Lagrangian tool developed here and a comparison with more traditional Eulerian diagnoses of the coupled interactions of the atmosphere and ocean.

Acknowledgements We would like to thank Y. Huang, T. M. Merlis, and B. Tremblay for their useful discussions and comments, and we gratefully acknowledge B. Dattore from NCEP for providing reanalysis data and A. Stohl and his team for making FLEXPART code available. Funding for this work was provided by the NSERC Discovery Program, FQRNT's Programme Établissement de Nouveaux Chercheurs Universitaires, and Québec-Océan. We would also like to thank two anonymous reviewers who helped us to improve this paper.

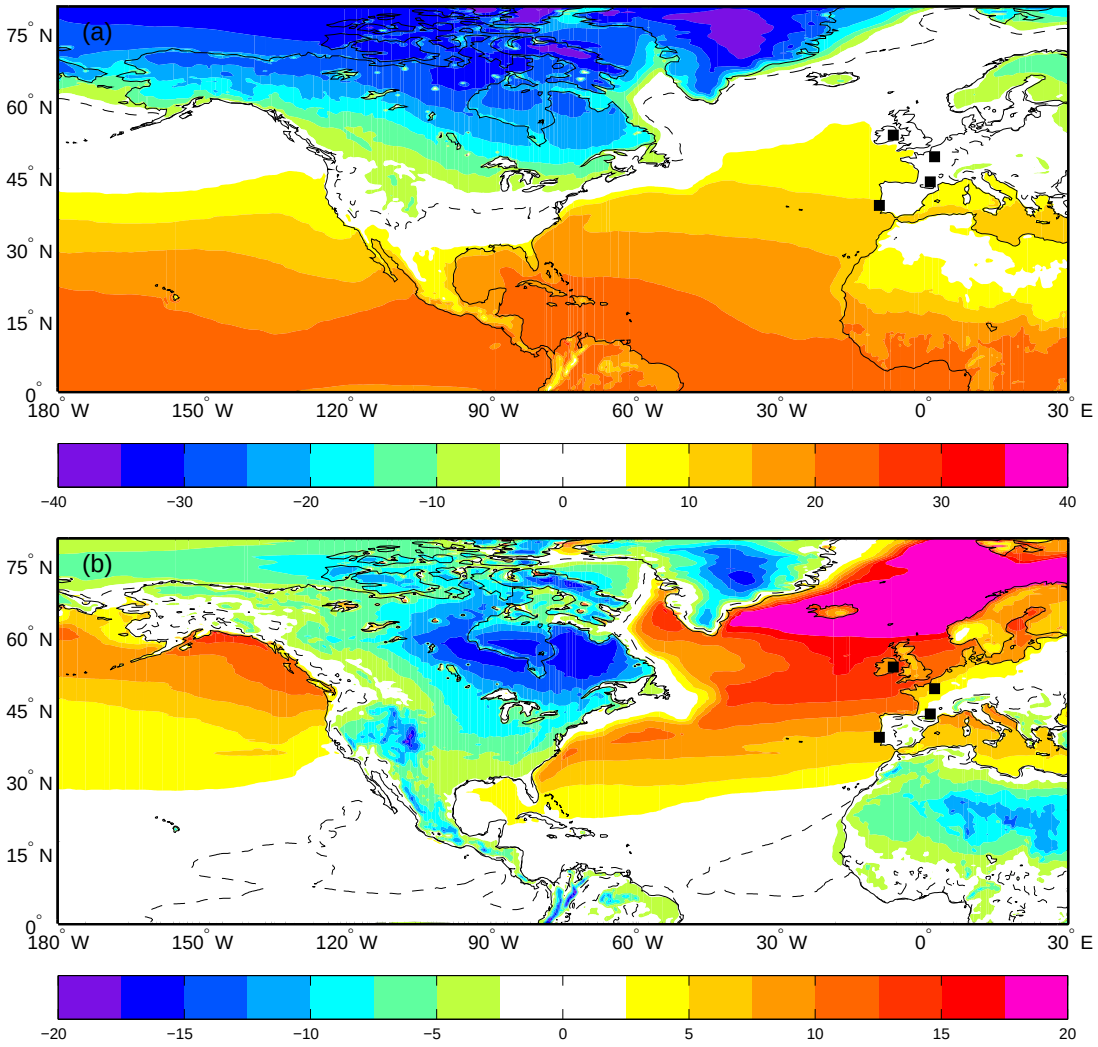

Fig. 1 a) January mean surface temperature [°C] (sea surface temperature over the ocean and surface air temperature over the land) for 1981 to 2009, and b) deviation of the surface temperature from the zonal mean [°C] for the same period, both constructed with NCEP CFSR datasets. The black dashed lines denote the 0 °C contour in each plot, while the black squares represent the locations of four western European cities investigated in this study.

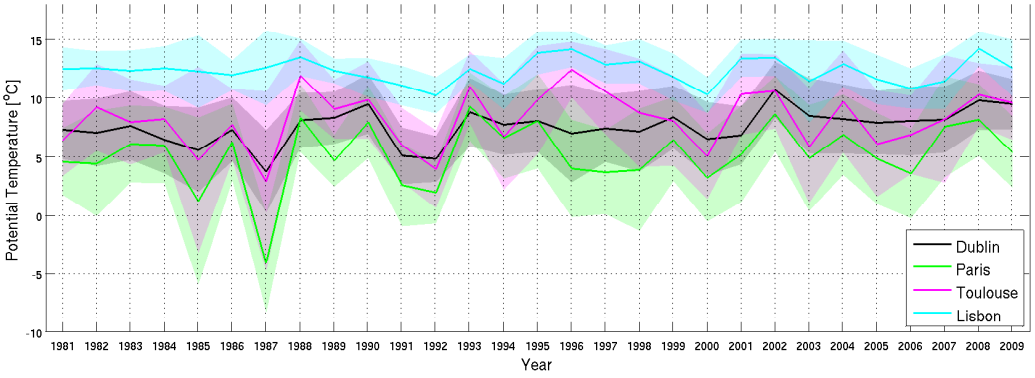

Fig. 2 Time series of January potential temperature in the four western European cities we investigate in this study. The solid lines denote the mean values, while the envelops surrounding the solid lines indicate the monthly standard deviation in each city.

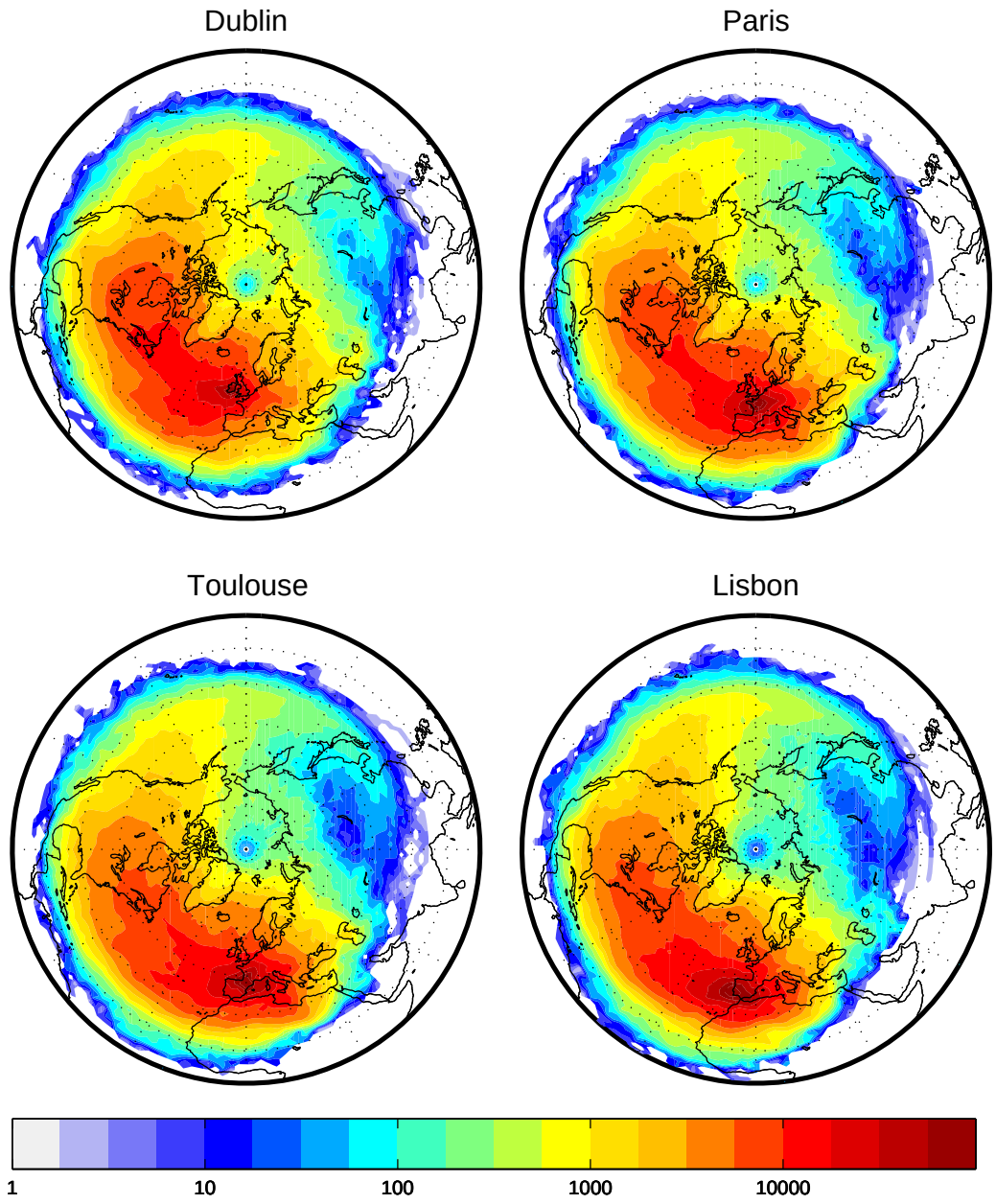

Fig. 3 Number density of the hourly particle positions computed by counting the number of particles that pass through each 2° × 2° grid cell for the 29 simulated Januaries. Note that the colorbar is given in a log 10 scale.

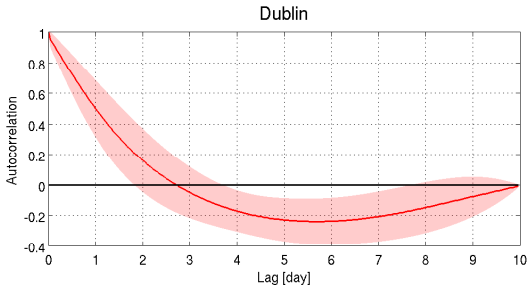

Fig. 4 The mean autocorrelation function of January potential temperature along the trajectories (solid line) and its one standard deviation (shading) for Dublin. The Lagrangian decorrelation timescale is taken as the first zero crossing of the function. The other three cities shared similar results to Dublin (not shown).

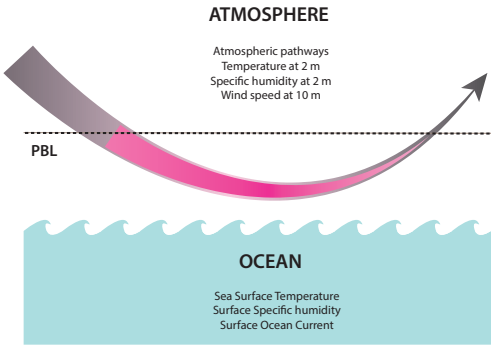

Fig. 5 A schematic of our methodology, calculating turbulent fluxes with bulk formulae along the established trajectories. The grey line indicates one atmospheric particle trajectory. When its hourly position falls within planetary boundary layer (the top of PBL indicated by the black dashed line), we compute the turbulent fluxes using the atmospheric and oceanic variables separately listed in the figure. The part of the trajectory where we conduct this operation is highlighted by the magenta line. The atmospheric variables include atmospheric pathway locations, surface air temperature and moisture at 2 m, and wind speed. The oceanic variables include the sea surface temperature, surface specific humidity and surface currents.

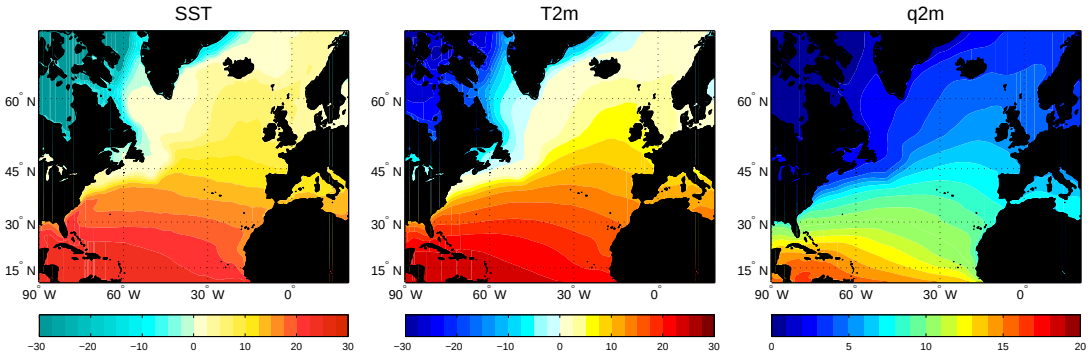

Fig. 6 The 29-year average January sea surface temperature (SST) [°C] (left), atmospheric surface temperature at 2 m above sea level (T2m) [°C] (middle), and specific humidity at 2 m above sea level (q2m) [g/kg] (right) over the North Atlantic, which are used in *PathVAR*, *AtmVAR*, and *PathSSTVAR* simulations.

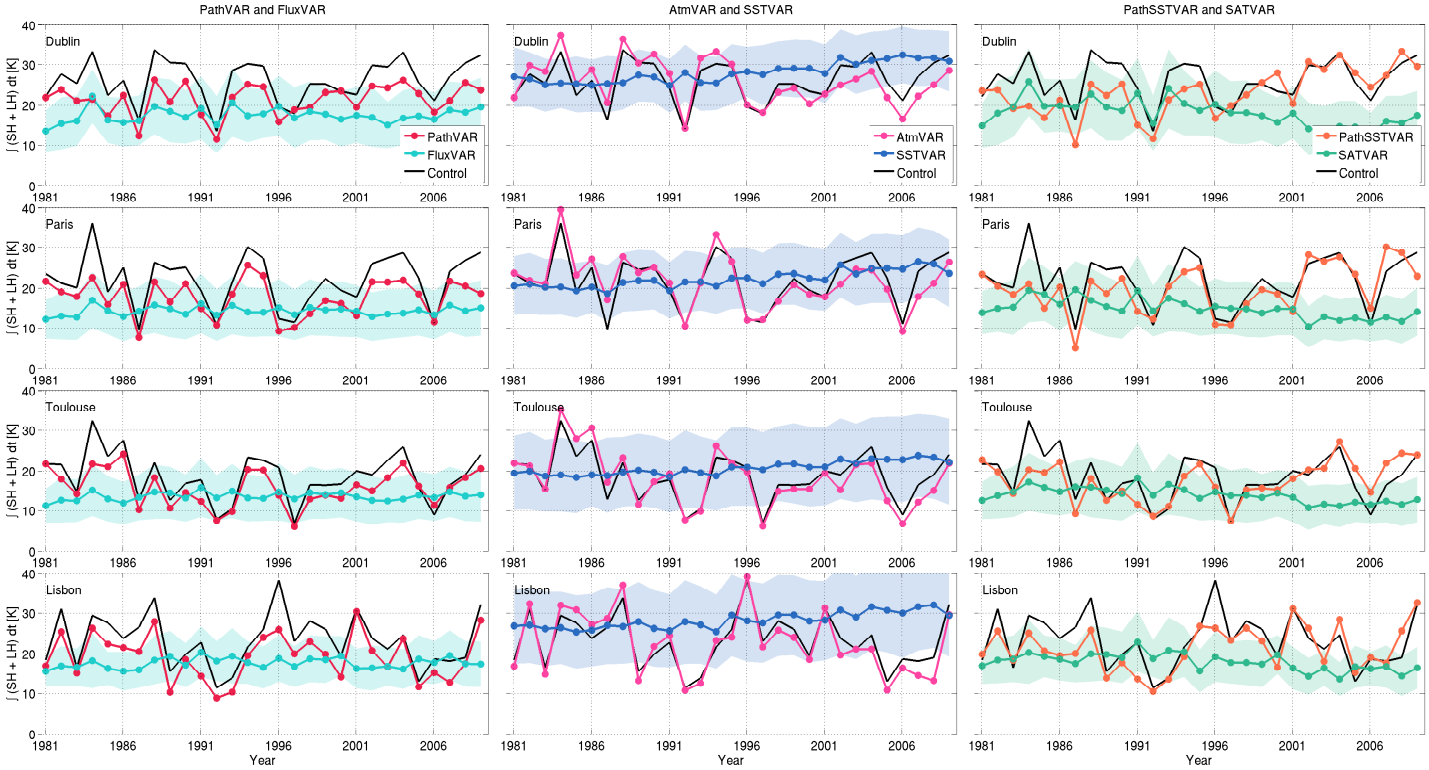

Fig. 7 Time series of the mean January surface heat fluxes (SH + LH) integrated over 10 days along the atmospheric trajectories for the six idealised simulations (coloured lines) for four western European cities summarised in Table 2. The rows represent the results for each city: Dublin (top row), Paris (second row), Toulouse (third row), and Lisbon (last row). The columns give the results for pairs of idealised simulations: *PathVAR* and *FluxVAR* (first column), *AtmVAR* and *SSTVAR* (second column), and *PathSSTVAR* and *SATVAR* (last column). The mean integrated heat fluxes of the *Control* simulation is repeated by the black solid line in every plot. The light-shaded envelopes for *FluxVAR*, *SSTVAR*, and *SATVAR* denote two standard deviations of ensemble of ten simulations. SH flux is expressed as the temperature change induced in the atmospheric particle due to a given flux [K], and likewise, LH is given as the temperature change induced in the particle upon condensation of all the moisture gained from the turbulent exchange with the ocean [K]. The correlation coefficient of each simulation and *Control* is given in Table 3.

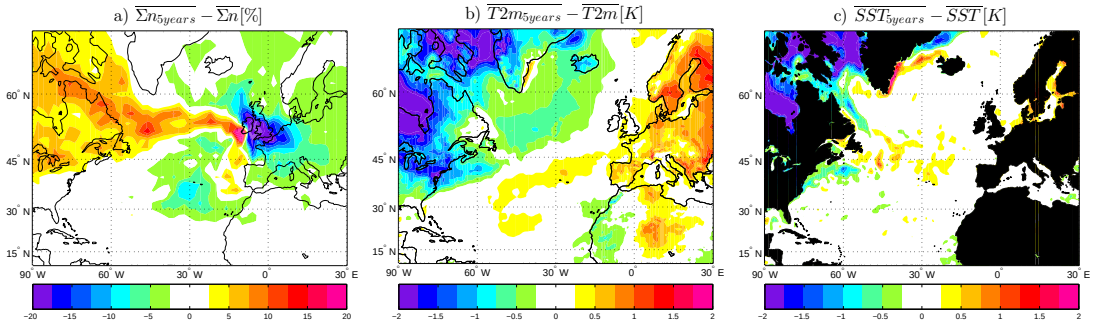

Fig. 8 Anomalous conditions during the years in which *PathVAR* most underestimates the true turbulent fluxes (simulated in *Control*). Each panel is made by subtracting the 29-year climatological mean conditions from the mean of the 5 years during which *PathVAR* most underestimates the fluxes relative to *Control* for Dublin (year 1984, 1988, 1989, 2004, and 2009; see Figure 7). Differences are in a) particle number density [%] (i.e. the percentage of total particles in each 2° × 2° grid cell in the 5-year composite ($\overline{\Sigma n_{5years}}$) minus the percentage of total particles in each grid cell for the 29 year climatology($\overline{\Sigma n}$)), b) surface air temperature at 2 m above sea level (T2m) [°C], and c) SST [°C].

	$\int(SH+LH)dt$ vs. $\int \frac{D\theta}{Dt}dt$	$\int(SH+LH)dt+\theta_i$ vs. θ_f
Dublin	0.94*	0.87*
Paris	0.94*	0.90*
Toulouse	0.87*	0.59*
Lisbon	0.90*	0.79*

Table 1 Correlation coefficients constructed with January averages of the ten day accumulated temperature change ($\int \frac{D\theta}{Dt}dt = \theta_f - \theta_i$), the ten day accumulated turbulent fluxes from bulk parametrisation ($\int(SH+LH)dt$), and initial and final potential temperature (θ_i, θ_f), where the final temperature is the western European cities. The starred values represent the statistically significant results at 95% confidence level.

Simulation Name	Variable	Fixed
PathVAR	Paths	Fluxes
FluxVAR	Fluxes	Paths
AtmVAR	Paths & T2m & q2m	SST
SSTVAR	SST	Paths & T2m & q2m
PathSSTVAR	Paths & SST	T2m & q2m
SATVAR	T2m & q2m	Paths & SST

Table 2 Three pairs of simulations designed to elucidate the control of each variable in the resultant heat flux variabilities. "Path" stands for atmospheric pathways, "Fluxes" stands for the turbulent fluxes (SH and LH), "SAT" stands for surface atmospheric temperature (T2m) and specific humidity at 2 m above sea level (q2m). "Atm" stands for atmospheric properties (atmospheric pathways + air temperature and specific humidity at 2 m), and SST stands for sea surface temperature.

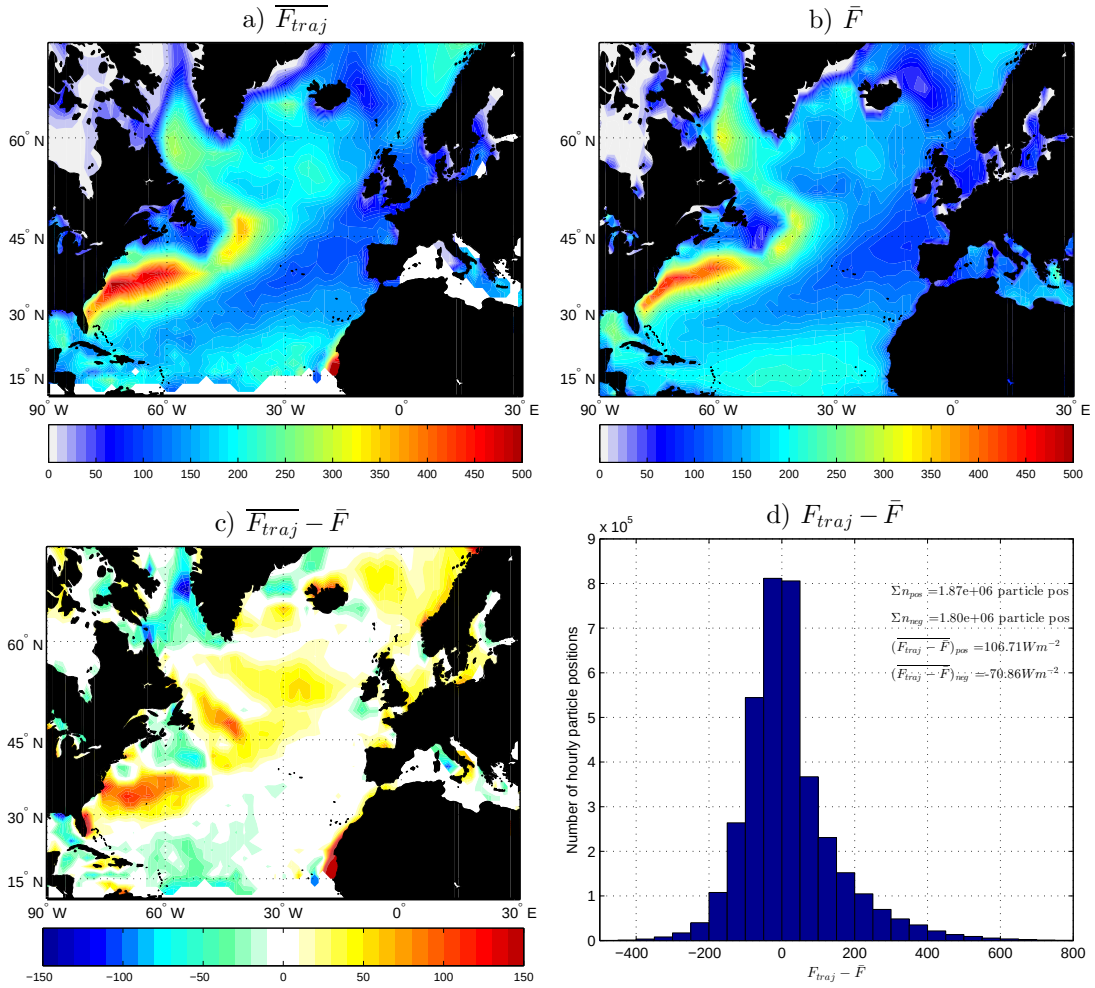

Fig. 9 Turbulent fluxes over the North Atlantic. a) Mean sensible heat + latent heat averaged along the trajectories to Dublin for all 29-year releases in *Control* in W m^{-2} ($\overline{F_{traj}}$). b) Eulerian mean heat fluxes ($\bar{F}$) over the 29 year NCEP CFSR climatology in W $^{-2}$. c) $\overline{F_{traj}}$ - $\bar{F}$ (i.e. Panel a minus Panel b) in W m^{-2}. d) Histogram of the difference between fluxes (SH + LH) for individual particles (F_{traj}) at each instantaneous position minus the 29-year climatological mean flux in a grid cell containing that position ($\bar{F}$). $(\overline{F_{traj} - \bar{F}})_{pos}$ and $(\overline{F_{traj} - \bar{F}})_{neg}$ represent the mean of all fluxes for particles in which, $F_{traj} - \bar{F}$, is greater than zero and less than zero, respectively. Σn_{pos} and Σn_{neg} are the numbers of hourly trajectory positions that have $F_{traj} - \bar{F}$ greater than zero and less than zero, respectively.

References

Alexander MA, Halimeda Kilbourne K, Nye JA (2014) Climate variability during warm and cold phases of the Atlantic Multidecadal Oscillation (AMO) 1871-2008. Journal of Marine Systems 133:14–26, DOI 10.1016/j.jmarsys.2013.07.017

Arguez A, O'Brien JJ, Smith SR (2009) Air temperature impacts over Eastern North America and Europe associated with low-frequency North Atlantic SST variability. International Journal of

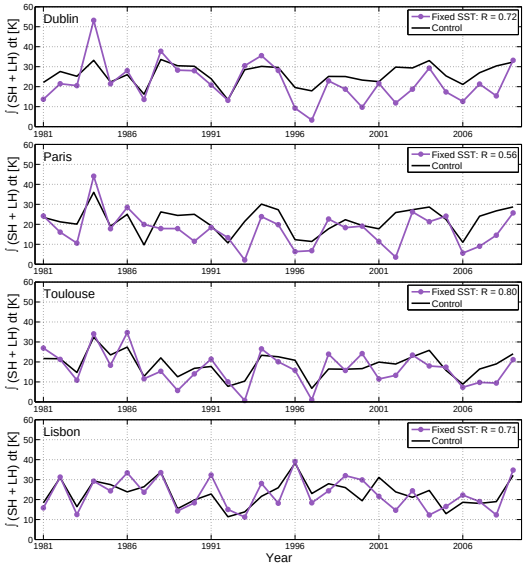

Fig. 10 Time series of surface heat fluxes (SH + LH) integrated over the 10 days along the atmospheric trajectories for *UniformSST* simulation, in which we use the varying atmospheric components (atmospheric trajectory positions, T2m, q2m, and wind speed), but set the SST to the uniform value equal to the mean SST value sampled by atmospheric particles back tracked from each city (7.5°C for Dublin, 7.3°C for Paris, 9.4°C for Toulouse, and 11.8°C for Lisbon). The black solid line in each plot is the result of the *Control* simulation, while the purple lines indicate that of *UniformSST* simulations. The correlation coefficient between *UniformSST* and *Control* for each city is indicated in each box, and all four cities are statistically significant correlations at 95% confidence level.

Simulation Name	Dublin	Paris	Toulouse	Lisbon
$PathVAR$	0.85*	0.92*	0.92*	0.92*
$FluxVAR$	0.34	0.20	-0.07	-0.07
$AtmVAR$	0.83*	0.90*	0.94*	0.96*
$SSTVAR$	0.06	0.18	-0.11	-0.06
$PathSSTVAR$	0.69*	0.81*	0.77*	0.79*
$SATVAR$	0.14	-0.11	0.04	0.01

Table 3 Correlation coefficient of the January-averaged accumulated turbulent heat fluxes ($\int(SH + LH)dt$) in each idealised simulation with the fluxes from *Control*. The starred values represent the statistically significant correlations at 95% confidence level.

Simulation Name	Dublin	Paris	Toulouse	Lisbon
$PathVAR$	5.41	5.08	3.64	4.63
$FluxVAR$	9.74	9.85	7.82	8.85
$AtmVAR$	3.13	2.92	2.36	2.46
SSTVAR	5.77	6.27	6.62	8.50
$PathSSTVAR$	5.14	4.35	3.92	4.42
$SATVAR$	9.59	9.89	7.59	8.64

Table 4 Root mean square errors [K] of the January-averaged accumulated turbulent heat fluxes ($\int(SH+LH)dt$) in each idealised simulations calculated relative to *Control*.

Climatology 29:1–10

Bjerknes J (1964) Atlantic Air-Sea Interaction. In: Landsberg HE, Van Mieghem J (eds) Advances in Geophysics, Academic Press, New York, London, pp 1–82

Blender R, Luksch U, Fraedrich K, Raible CC (2003) Predictability study of the observed and simulated European climate using linear regression. Quarterly Journal of the Royal Meteorological Society 129:2299–2313, DOI 10.1256/qj.02.103

Booth BBB, Dunstone NJ, Halloran PR, Andrews T, Bellouin N (2012) Aerosols implicated as a prime driver of twentieth-century North Atlantic climate variability. Nature 484(7393):228–232, DOI 10.1038/nature10946

Buckley MW, Ponte RM, Forget G, Heimbach P (2014) Low-frequency SST and upper-ocean heat content variability in the North Atlantic. Journal of Climate 27:4996–5018, DOI 10.1175/JCLI-D-13-00316.1

Decker M, Brunke MA, Wang Z, Sakaguchi K, Zeng X, Bosilovich MG (2012) Evaluation of the Reanalysis Products from GSFC, NCEP, and ECMWF Using Flux Tower Observations. Journal of Climate 25(6):1916–1944, DOI 10.1175/JCLI-D-11-00004.1

Dong B, Sutton RT, Woollings T, Hodges K (2013) Variability of the North Atlantic summer storm track: mechanisms and impacts on European climate. Environmental Research Letters 8(3):034,037, DOI 10.1088/1748-9326/8/3/034037

Dong S, Kelly KA (2004) Heat Budget in the Gulf Stream Region: The Importance of Heat Storage and Advection. Journal of Physical Oceanography 34(5):1214–1231

Dong S, Hautala SL, Kelly KA (2007) Interannual Variations in Upper-Ocean Heat Content and Heat Transport Convergence in the Western North Atlantic. Journal of Physical Oceanography 37(11):2682–2697, DOI 10.1175/2007JPO3645.1

Enfield DB, Mestas-Nunez AM, Trimble PJ (2001) The Atlantic multidecadal oscillation and its relation to rainfall and river flows in the continental U.S. Geophysical Research Letters 28(10):2077–2080

Fairall CW, Bradley EF, Rogers DP, Edson JB, Young GS (1996) Bulk parameterization of air-sea fluxes for Tropical Ocean- Global Atmosphere Coupled-Ocean Atmosphere Response Experiment difference relative analysis. Journal of Geophysical Research 101:3747–3764

Fairall CW, Bradley EF, Hare JE, Grachev AA, Edson JB (2003) Bulk Parameterization of Air-Sea Fluxes: Updates and Verification for the COARE Algorithm. Journal of Climate pp 571–591

543 Gámiz-Fortis SR, Esteban-Parra MJ, Pozo-Vázquez D, Castro-Díez Y (2011) Variability of the
544 monthly European temperature and its association with the Atlantic sea-surface temperature
545 from interannual to multidecadal scales. International Journal of Climatology 31(14):2115–2140,
546 DOI 10.1002/joc.2219
547 Gulev SK, Latif M, Keenlyside N, Park W, Koltermann KP (2013) North Atlantic Ocean control on
548 surface heat flux on multidecadal timescales. Nature 499(7459):464–7, DOI 10.1038/nature12268
549 Häkkinen S, Rhines PB, Worthen DL (2011) Atmospheric blocking and Atlantic multidecadal ocean
550 variability. Science (New York, NY) 334(6056):655–9, DOI 10.1126/science.1205683
551 Hodges KI, Lee RW, Bengtsson L (2011) A Comparison of Extratropical Cyclones in Recent Reanal-
552 yses ERA-Interim, NASA MERRA, NCEP CFSR, and JRA-25. Journal of Climate 24(18):4888–
553 4906, DOI 10.1175/2011JCLI4097.1
554 Johns WE, Baringer MO, Beal LM, Cunningham SA, Kanzow T, Bryden HL, Hirschi JJM,
555 Marotzke J, Meinen CS, Shaw B, Curry R (2011) Continuous, Array-Based Estimates
556 of Atlantic Ocean Heat Transport at 26.5N. Journal of Climate 24(10):2429–2449, DOI
557 10.1175/2010JCLI3997.1
558 Junge MM, Stephenson DB (2003) Mediated and direct effects of the North Atlantic Ocean on
559 winter temperatures in northwest Europe. International Journal of Climatology 23(3):245–261,
560 DOI 10.1002/joc.867
561 Kushnir Y (1994) Interdecadal variations in North Atlantic sea surface temperature and associated
562 atmospheric conditions. Journal of Climate 7:141–157
563 Maryon RH (1998) Determining cross-wind variance for low frequency wind meander. Atmospheric
564 Environment 32(2):115–121
565 Maury MF (1860) The physical geography of the sea, and its meteorology. Harper & Brothers,
566 New York
567 McCarthy G, Frajka-Williams E, Johns WE, Baringer MO, Meinen CS, Bryden HL, Rayner D,
568 Duchez A, Roberts C, Cunningham SA (2012) Observed interannual variability of the At-
569 lantic meridional overturning circulation at 26.5N. Geophysical Research Letters 39(19), DOI
570 10.1029/2012GL052933
571 Orlanski I (1998) Poleward Deflection of Storm Tracks. Journal of the Atmospheric Sciences
572 55:2577–2602
573 Peixoto JP, Oort AH (1992) Physics of climate. American Institute of Physics, New York

Rhines PB, Häkkinen S, Josey SA (2008) Is Oceanic Heat Transport Significant in the Climate System? In: Dickson RR, Meincke J, Rhines PB (eds) Arctic-Subarctic Ocean Fluxes: Defining the role of the Northern Seas in Climate, Springer Verlag, New York, chap 4

Rudeva I, Gulev SK (2011) Composite Analysis of North Atlantic Extratropical Cyclones in NCEP-NCAR Reanalysis Data. Monthly Weather Review 139(5):1419–1446, DOI 10.1175/2010MWR3294.1

Saha S, Moorthi S, Pan HL, Wu X, Wang JW, Nadiga S, Tripp P, Kistler R, Woollen J, Behringer D, Liu H, Stokes D, Grumbine R, Gayno G, Wang J, Hou YT, Chuang HY, Juang HMH, Sela J, Iredell M, Treadon R, Kleist D, Van Delst P, Keyser D, Derber J, Ek M, Meng J, Wei H, Yang R, Load S, Van Den Dool H, Kumar A, Wang W, Long C, Chelliah M, Xue Y, Huang B, Schemm JK, Ebisuzaki W, Lin R, Xie P, Chen M, Zhou S, Higgins W, Zou CZ, Liu Q, Chen Y, Han Y, Cucurull L, Reynolds RW, Rutledge G, Goldberg M (2010) The NCEP climate forecast system reanalysis. Bulletin of the American Meteorological Society 91(August):1015–1057, DOI 10.1175/2010Bams3001.1

Seager R, Battisti DS, Yin J, Gordon N, Naik N, Clement AC, Cane MA (2002) Is the Gulf Stream responsible for Europe's mild winters? Quarterly Journal of the Royal Meteorological Society 128(586):2563–2586, DOI 10.1256/qj.01.128

Stohl A, Thomson DJ (1999) A density correction for Lagrangian particle dispersion models. Boundary-Layer Meteorology 90:155–167

Stohl A, Forster C, Frank A, Seibert P, Wotawa G (2005) Technical note: The Lagrangian particle dispersion model FLEXPART version 6.2. Atmospheric Chemistry and Physics 5:2461–2474

Sutton RT, Dong B (2012) Atlantic Ocean influence on a shift in European climate in the 1990s. Nature Geoscience 5(11):788–792, DOI 10.1038/ngeo

Tilinina N, Gulev SK, Rudeva I, Koltermann P (2013) Comparing Cyclone Life Cycle Characteristics and Their Interannual Variability in Different Reanalyses. Journal of Climate 26(17):6419–6438, DOI 10.1175/JCLI-D-12-00777.1

Trenberth KE, Caron JM (2001) Estimates of meridional atmosphere and ocean heat transports. Journal of Climate 14:3433–3443

Vogelezang DHP, Holtslag AAM (1996) Evaluation and model impacts of alternative boundary-layer height formulations. Boundary-Layer Meteorology 81:245–269

Woollings T, Gregory JM, Pinto JG, Reyers M, Brayshaw DJ (2012) Response of the North Atlantic storm track to climate change shaped by ocean-atmosphere coupling. Nature Geoscience 5(5):313–317, DOI 10.1038/ngeo1438

Wunsch C, Heimbach P (2007) Practical global oceanic state estimation. Physica D: Nonlinear Phenomena 230(1-2):197–208, DOI 10.1016/j.physd.2006.09.040

Yasuda T, Hanawa K (1997) Decadal Changes in the Mode Waters in the Midlatitude North Pacific. Journal of Physical Oceanography 27(6):858–870

Yulaeva E, Schneider N, Pierce DW, Barnett TP (2001) Modeling of North Pacific climate variability forced by oceanic heat flux anomalies. Journal of Climate 14:4027–4046